Dexterity in Robotic Grasping – Object Oscillation

José Maria Rosa Alves
jose.alves@tecnico.ulisboa.pt

Instituto Superior Técnico – Universidade de Lisboa, Lisboa, Portugal

December 2021

Abstract - This thesis covers the underlying mechanisms of grasping and an oscillating system. It uses impedance control methods to stabilize the system and reach a cyclical behavior where an object, a pen, is oscillated by two robotic fingers. A bio-inspired perception system is employed for the detection of the position of the object, in relation to the robotic hand, which in turn uses this information for its manipulation. Such detection is obtained via the forces and position of said forces on the fingertips of the robotic system. Through the system's perception of the position of its fingertips and the aforementioned detection of the pen's position, an impedance control method was put forward, through the control of the grasping force and the following of a sinusoidal reference for the object's trajectory. Further, the analysis of the system allowed to show the presence of a resonant frequency at which the oscillation magnitude of the object could be maximized. The system's response is discussed for a range of frequencies. At higher frequencies, the phenomenon of period doubling is made evident, where a new periodic trajectory emerges from the existing periodic trajectory at which the pen had been moving thus far.

Keywords: Bioinspired grasping, Cyclical behavior, Impedance control, Impedance of grasping, Oscillating system.

1 INTRODUCTION

The act of object grasping is quite a complex ability, unique to some select few in the animal kingdom [1] and without a doubt the most important trait that allowed for the evolution of *Homo sapiens*, humans, as we know them today. It allowed early primates to take up tool use [2] and to control fire [3, 4], two defining abilities that mark the start of the human era. Grasping is not easy, which is reflected on the abundance, or lack thereof, of this ability in the wild [2]. This technique proves very worthwhile, though the combination of high dexterity and intelligence is often prohibitive to many, it rewards greatly those who master it [5] with a rapid ascension in the food chain hierarchy. This ability was used by ancient humans for tool making [6, 7] and it took up a big part of their time, where the ability to grasp and work the tool were crucial for survivability.

1.1 Motivation

The motivation behind this essay lies on the drive to better understand the art of grasping and the ability for complex hand maneuvers. How this knowledge could be applied to robotics or possibly prosthetics, where a mechanical system need be able to execute the fluid yet complex movements a human can do with ease, almost without any critical thinking behind it.

Contemporary uses of grasping in robotic handling generally consist of holding the grasped object steady and firmly to manipulate it [8, 9, 10]. In these cases, the robot does not consider motion decoupled from the object being manipulated. This work attempts to use the mix of quick movements and impedance control to dynamically manipulate and oscillate an object, and to act as an inspiration for further development in the dynamic manipulation of objects.

1.2 Objective and Methods

The goal of this study is to build a biologically inspired model of a robotic hand and a controller capable of handling a pen through complex motion, specifically the ability to wiggle the pen on the fingertips, making an oscillating cycling motion. The model must reflect its biological counterparts regarding the sensing and the signal propagation of the system. Additionally, the controller should be robust regarding the system's operating characteristics and outside factors that might disturb the well-functioning of the system.

Towards this goal, such model was constructed, and an impedance-based control was implemented at the level of grasping and object maneuverability, while position control was implemented at the level of the positioning of the fingers. The system's response is then thoroughly discussed and analyzed so as to evaluate its stability, robustness and cyclicity.

2 MODEL

The geometric hypotheses for the model are that the problem can be simplified as a 2-D task, both fingertips are identical, of circular geometry, the pen is cylindrical and perfectly straight, and the contact occurs in a singular point on the bodies. Given these, a kinematic model for each body was created. For ease of writing, the pen will be referenced as body 1 and the upper fingertip and lower fingertip as body 2 and 2′ respectively in this document. Below, in Figure 2.1,

the pen's model is illustrated. In Figure 2.2 the robotic hand's model is illustrated, where its construction is displayed.

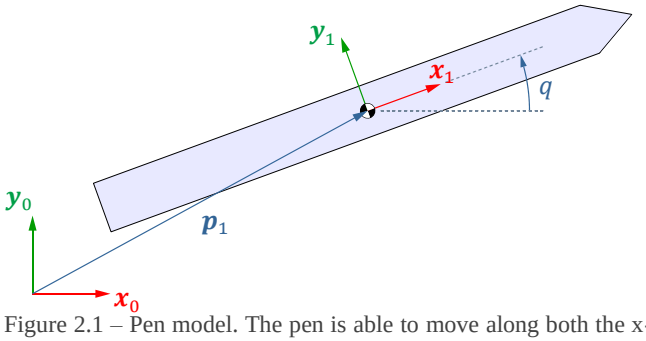

Figure 2.1 – Pen model. The pen is able to move along both the x-axis and y-axis and is able to rotate around the z-axis and its rotation is given by the angle q. Its reference frame is numerated with the number 1.

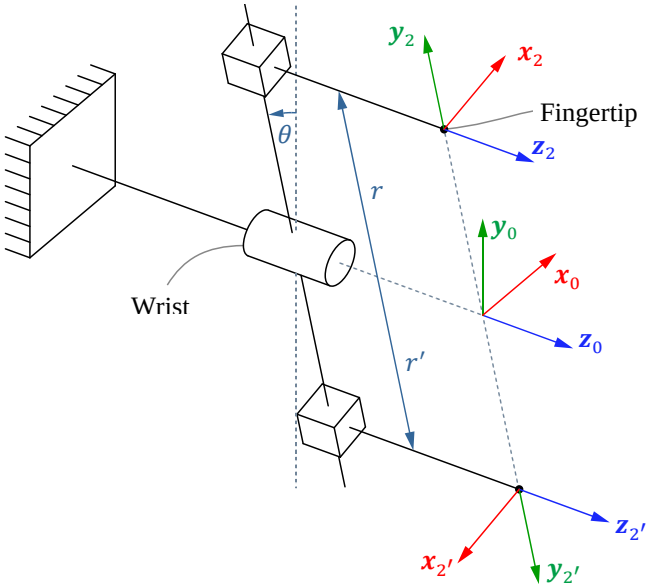

Figure 2.2 – Robotic hand model. The wrist joint is represented as a cylinder, conveying a rotation between the fixed base and the fingertips by an angle θ. The fingertips have their respective frames of reference attached to them, namely 2 and 2′. Their displacement from the rotation axis, z_0, is measured along y_2 and y_2', as noted by r and r'.

Table 1 – Parameters of the dynamic models. The finger corresponds to the full finger, including the fingertip and the finger body, moved by the prismatic joint. The inertia that of the body's z-axis, at its center of mass. The center of mass is in relation to the geometric center of the object, in the 2-D plane considered in this document.

	Mass $[g]$	Inertia $[g\ mm^2]$	Center of mass $[mm]$
Pen	4.5	7099.9	$[0 \quad 0 \quad 0]^T$
Finger	16.3	1651.7	$[0 \quad 0 \quad 55.55]^T$
Base	158.7	17584.0	$[0 \quad 0 \quad 0]^T$

The pen's center of mass and geometric center match, and the pen has a length of 132 mm and a diameter of 8 mm. The fingertip's center of mass and geometric center also match and the fingertip has a radius of 8.89 mm. In Table 1, the dynamic parameters of the models are gathered.

2.1 Simulation environment

The environment consists of the two subsystems, the robotic hand and the pen. These are simulated in a virtual world that is affected by gravity, with a magnitude of 9.81 m/s^2 and the negative direction of the y-axis.

2.2 Contact

The contact is defined using a penetration distance, δ, that measures the penetration of the bodies on each other. By using the position and velocity of the pen and the fingertips, and δ, it is possible to obtain the forces that would result from the contact between them.

2.2.1 Normal force

The normal force, F_n, from [11], is given by

$$F_n = \begin{cases} -K\,\delta^a, & \delta \geq 0 \\ 0, & \text{otherwise.} \end{cases} \tag{2.1}$$

where a is a geometry exponent and K can be calculated by the expression

$$K = \begin{cases} k\left(1 + \frac{\dot{\delta}}{\dot{\delta}_-}\beta\right), & \dot{\delta} \geq -\varepsilon\dot{\delta}_- \\ k(1-\beta\varepsilon)\exp\left(\frac{\beta}{1-\beta\varepsilon}\frac{\dot{\delta}+\varepsilon\dot{\delta}_-}{\dot{\delta}_-}\right), & \text{otherwise.} \end{cases} \tag{2.2}$$

where k is the nonlinear stiffness coefficient of the collision ($k = 2 \times 10^5$), $\dot{\delta}_-$ is the value of $\dot{\delta}$ right before impact, ε is the restitution coefficient and β is the inverse restitution.

2.2.2 Friction force

The friction force can be split into two states, the static friction state, when the objects are in adhesion, and the dynamic friction state, when the objects slide over one another. The transition between these states is detailed in Figure 2.3. This system was adapted from [12]. The transition from sliding to adhesion occurs when contact velocities are very small [13], and the transition from adhesion to sliding occurs when the static friction force overcomes the allowable force as per Coulomb's friction law [13, 14].

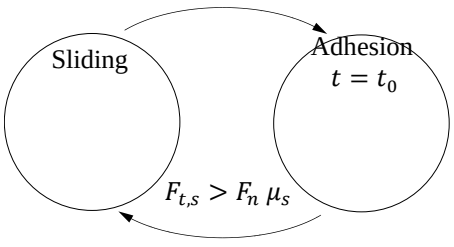

Figure 2.3 – State machine of the friction force. The system begins at the sliding state. Coefficients μ_s and μ_d adapted from [14, 15].

The contact transitions to adhesion if the tangential velocity between the bodies, v_x, is lower than some limit v_{lim}. The transition from adhesion to sliding occurs when the normal force, F_n, multiplied by the static coefficient μ_s is lower than the static friction force $F_{t,s}$.

2.2.2.1 Static friction (Adhesion)

The static friction, $F_{t,s}$, is modeled as a strictly adhesive force, following [11], as

$$F_{t,s} = -K_s\, s_x \exp(\eta \tanh(\gamma\, s_x)\, v_x). \qquad (2.3)$$

compromising a nonlinear spring, with stiffness K_s, and a nonlinear damping, η, where s_x is the spring's displacement, v_x the spring's velocity and γ a smoothing constant. The spring's displacement, s_x, is calculated from v_x by integration, from the time at which adhesive contact beings, t_0, to $t > t_0$ the time during the contact event. The initial spring's displacement, $s_x(t_0)$, is the displacement equivalent to the dynamic friction force, from the transition

$$s_x(t) = \int_{t_0}^{t} v_x(u)du + s_x(t_0). \qquad (2.4)$$

2.2.2.2 Friction force (Sliding)

The dynamic friction was modeled following Coulomb's friction law [13], such that the friction force is given as

$$F_{t,d} = -\text{sign}(v_x)\, F_n\, \mu_d, \qquad (2.5)$$

where μ_d is the dynamic coefficient [15]. The initial spring's displacement, $s_x(t_0)$, mentioned earlier, is calculated by establishing continuity between the adhesion and sliding friction forces, $F_{t,d} = F_{t,s}$, such that with $v_x < v_{lim} \sim 10^{-3}$, it is calculated as

$$s_x(t_0) = \frac{F_{t,d}}{K_s}. \qquad (2.6)$$

3 PHYSIOLOGY OF THE HUMAN TOUCH – PERCEPTION

With the purpose of creating a bio-inspired controller for the hand, it is important for the perception of the model to also be nature-like and to follow the physiological limits of a human hand. It therefore is essential to know the intricacies of the human touch, which means getting to know the mechanoreceptors in the fingertips and in the relevant muscles, in order to replicate their behavior. The following was gathered from [16].

3.1 Skin mechanoreceptors

A mechanoreceptor is a sensory receptor that responds to mechanical pressure or distortion. There are several types of these sensors within the human skin. This document focuses on the study of the mechanoreceptors located in glabrous (hairless) mammalian skin, which is the skin present in the fingertips of primates and other mammals similar to humans. There are four main types of mechanoreceptors in the skin region, from which three will be discussed, namely Meissner corpuscles, Merkel cells and Ruffini endings.

3.1.1 Meissner corpuscles

The Meissner corpuscle is a rapid adapting type 1 (close to skin surface) receptor, abbreviated as RA1. This corpuscle is responsible for sensitivity to light touch, slippage of objects and the detection of the texture of surfaces it encounters. The key features that the Meissner corpuscle would be able to integrate into the present model are then:

- Normal force;
- Tangential force.

3.1.2 Merkel cells

Merkel cells are slowly adapting type 1 receptors, abbreviated as SA1, located near the epidermis. They are responsible for detecting the amount of pressure applied on the skin and are particularly sensitive to edges, corners and points. Similarly to the Meissner corpuscle, they also play an important role in the detection of textures. The key features that the Merkel cells would be able to integrate into the present model are then:

- Position of contact with the finger and its rate of change.

3.1.3 Ruffini endings

Ruffini endings are slowly adapting type 2 receptors, SA2, that extend from the subcutaneous tissue to folds in the skin at the joints, in the palm or in the fingernails. These receptors are sensitive to the shape of large objects and can signal movements of the fingers and other joints due to stretch in the overlying skin. In combination with the muscle mechanoreceptors, mentioned in the next section, the key features that the Ruffini endings would be able to integrate into the present model are then:

- Position of finger;
- Position of the wrist.

3.2 Muscle mechanoreceptor: Muscle spindle

Muscle mechanoreceptors are sensory neurons located within the muscle. One of these, muscle spindles, are proprioceptors whose main function it is to provide information on muscle length and the rate of change of muscle length. These receptors run parallel to the muscle fibers. The key features that the muscle spindle would detect from the model are then:

- Position and velocity of the finger;
- Angle and angular velocity of the wrist.

3.3 Model variables usable from the model

It then follows that from the many sensory cells and mechanisms discussed above that there are a total of 14 state variables usable for the perception and control of the pen. Briefly, these are:

1. Angle between the pen and the upper finger ($\hat{\alpha}$);
2. Angle between the pen and the lower finger ($\hat{\alpha}'$);
3. Rate of change of the angle between the pen and the upper finger ($\dot{\hat{\alpha}}$);
4. Rate of change of the angle between the pen and the lower finger ($\dot{\hat{\alpha}}'$);
5. Tangential force felt by the upper finger ($\hat{F}_t$);
6. Normal force felt by the upper finger ($\hat{F}_n$);
7. Tangential force felt by the lower finger ($\hat{F}_t'$);
8. Normal force felt by the upper finger ($\hat{F}_n'$);
9. Upper finger's position ($\hat{r}$);
10. Lower finger's position ($\hat{r}'$);
11. Wrist's angle ($\hat{\theta}$);
12. Upper finger's velocity ($\dot{\hat{r}}$);
13. Lower finger's velocity ($\dot{\hat{r}}'$);
14. Wrist's angular velocity ($\dot{\hat{\theta}}$).

4 ESTIMATION OF THE PEN'S POSITION

In order to detect the pen's position, the estimator is assumed to know the dimensions, the mass and the inertia of the pen and finger. Moreover, for detection to take place, a normal force must be detected on the fingers, marking the pen's presence known. If no forces are detected in either finger, then the pen is not detected, resulting in its position being assumed to be where it was last detected at.

4.1 Angle estimation

The estimated angle of the pen $\hat{q}$ is calculated simply as the estimated angle of the wrist ($\hat{\theta}$) plus the estimated angle of contact ($\hat{\alpha}$),

$$\hat{q} = \hat{\theta} + \hat{\alpha}. \tag{4.1}$$

As the angle $\hat{\alpha}$ is only detected when there is contact with the pen, equation (4.1) is only valid when one of the fingers is in contact with the pen. By differentiating equation (4.1), the estimated pen's angular velocity is obtained as the sum of the angular velocity of the wrist and the contact's,

$$\dot{\hat{q}} = \dot{\hat{\theta}} + \dot{\hat{\alpha}}. \tag{4.2}$$

Due to the limitations of the sensory system, the angular acceleration of the wrist and the contact's is unknown and as such needs to be approximated. To do so, consider that there is a frequency at which the estimation of $\hat{\theta}$ and $\hat{\alpha}$ are precepted, in the muscle, [17, 18], and on the Merkel cells, [16], respectively. This frequency results in a time sample of 0.01 seconds, which can be used to estimate the angular acceleration, by subtracting the estimated angular velocity of the pen and the angular velocity estimated at a previous timestep and then dividing over the time sample, resulting in

$$\ddot{\hat{q}} = \frac{\dot{\hat{q}}_t - \dot{\hat{q}}_{t-1}}{T_s}. \tag{4.3}$$

4.2 Position estimation

Secondly, the position of the pen in relation to the fingers is estimated. To this end, the distance between the fingers is first calculated by using the angle at which the pen is felt on the finger ($\hat{\alpha}$) as follows.

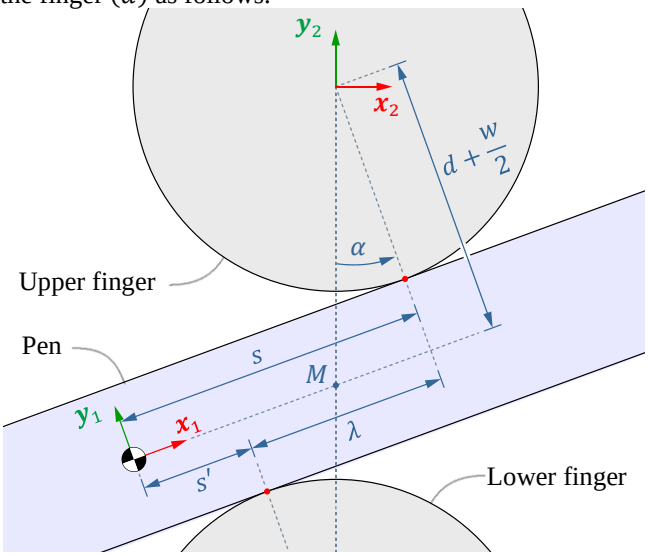

Figure 4.1 – Illustration of the pen between the fingers and definition of relevant variables for detection. The distance between the fingers, in the tangential direction of the pen, is given by λ. The x component of the distance from the pen's contact points to its center of mass, s and s' are defined. M is the intersection point between a line that joins the two fingers and the pen's x-axis, x_1.

As illustrated in Figure 4.1, the interfinger distance (λ) is estimated as

$$\lambda = 2\left(d + \frac{w}{2}\right)\tan(\hat{\alpha}). \tag{4.4}$$

Then, the forces felt on the fingers are used to estimate the forces affecting the pen, on the upper contact point

$$\hat{\boldsymbol{F}}_1 = \hat{\boldsymbol{R}}_2^1(-\hat{\boldsymbol{F}}_2), \tag{4.5}$$

and lower contact point

$$\hat{\boldsymbol{F}}_1' = \hat{\boldsymbol{R}}_{2'}^{1}(-\hat{\boldsymbol{F}}_2'). \tag{4.6}$$

These forces are used to estimate the distance they span from the center of mass of the pen by equating all the torques applied on the pen and its apparent rotation on the fingers. Towards this end, the distances from the upper finger and the lower finger to the center of mass of the pen, s and s', are first related to the interfinger distance, as

$$\hat{s} = \lambda + \hat{s}'. \tag{4.7}$$

Also, the position vectors for both contact points ($\hat{\boldsymbol{c}}_1$ and $\hat{\boldsymbol{c}}_1{}'$) on the pen are able to be estimated as

$$\hat{\boldsymbol{c}}_1 = \begin{bmatrix} \hat{s} & \frac{w}{2} & 0 \end{bmatrix}^T \tag{4.8}$$

and

$$\hat{\boldsymbol{c}}'_1 = \begin{bmatrix} \hat{s}' & -\frac{w}{2} & 0 \end{bmatrix}^T. \tag{4.9}$$

Then the torque balance can be equated, resulting in

$$I_{z,p}\,\ddot{\hat{q}} = \hat{\boldsymbol{c}}_1 \times \hat{\boldsymbol{F}}_1 + \hat{\boldsymbol{c}}'_1 \times \hat{\boldsymbol{F}}'_1. \tag{4.10}$$

where $I_{z,p}$ is the inertia of the pen. Now, introduction of equations (4.7), (4.8) and (4.9) into (4.10), results in

$$I_{z,p}\,\ddot{\hat{q}} = -\hat{F}_t\,\frac{w}{2} + \hat{F}_n\,\hat{s} - \hat{F}'_t\left(-\frac{w}{2}\right) + \hat{F}_i \tag{4.11}$$

and the distance from the fingers to the center of mass can be solved as

$$\begin{cases} \hat{s}' = \dfrac{I_{z,p}\ddot{\hat{q}} + \frac{w}{2}\hat{F}_t - \lambda\,\hat{F}_n - \frac{w}{2}\hat{F}'_t}{\hat{F}_n - \hat{F}'_n}, \\ \hat{s} = \lambda + \hat{s}'. \end{cases} \tag{4.12}$$

With the distances between the center of mass and each finger calculated, the distance between the mass center and point M can now be calculated as the average of both distances, in the opposite direction. Thus, the displacement from point M towards the mass center can be estimated, in the world frame, as

$$\hat{\boldsymbol{r}}_{M,1} = \hat{\boldsymbol{R}}_1^0 \begin{bmatrix} -\left(\frac{\hat{s}+\hat{s}'}{2}\right) \\ 0 \\ 0 \end{bmatrix}. \tag{4.13}$$

The next step is to calculate the contribution of the fingers' position to the position of the pen's center of mass. Towards this end, a line is imagined connecting the fingers vertically, like done in Figure 4.2.

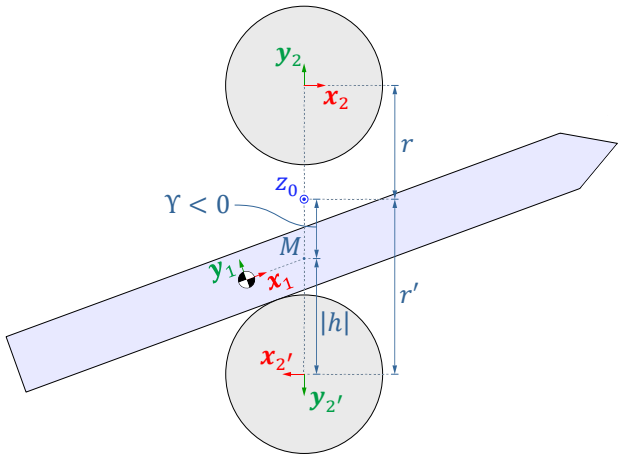

Figure 4.2 – A vertical dotted line connects the two fingers. The intersection between this line and the pen's x_1 axis is the point M, marked by a blue circle. $|\Upsilon|$ is the distance between the z_0 axis and point M and it is measured positively along y_2. The distance between M and the finger in contact with the pen is denoted as h.

Then the vertical distance from the point M to the axis z_0, Υ, is estimated, illustrated in Figure 4.2. In the simple case where both fingers are in contact with the pen, this height comes up to the average of the fingers' estimated distance to the wrist $\hat{r}$ and $\hat{r}'$, given as

$$\Upsilon = \frac{\hat{r} - \hat{r}'}{2}, \qquad \text{adjacent to both fingers.} \tag{4.14}$$

However, if the pen is only in contact with one of the fingers, as seen on Figure 4.2, Υ can be calculated as the distance h from the finger, calculated according to the Pythagoras' theorem as ($\delta \approx 0$)

$$h = \sqrt{\left(\frac{\lambda}{2}\right)^2 + \left(d + \frac{w}{2}\right)^2} \tag{4.15}$$

and the finger's distance to the wrist, $\hat{r}$,

$$\Upsilon = \begin{cases} \hat{r} - h, & \text{adjacent to upper fi} \\ h - \hat{r}', & \text{adjacent to lower fi} \end{cases} \tag{4.16}$$

Finally, the center of mass from the contribution of the fingers' position can be calculated as

$$\hat{\boldsymbol{r}}_{0,M} = \hat{\boldsymbol{R}}_2^0 \begin{bmatrix} 0 \\ \Upsilon \\ 0 \end{bmatrix} \tag{4.17}$$

The position of the center of mass of the pen is then the sum of both contributions in equations (4.13) and (4.17)

$$\hat{\boldsymbol{p}}_1 = \hat{\boldsymbol{r}}_{0,M} + \hat{\boldsymbol{r}}_{M,1}. \tag{4.18}$$

4.3 Validation

In order to estimate the pen's position through a simple exercise, the fingers were made to remain immobile and 16 centimeters apart (more than the pen's width). The pen was initialized with its center of mass at the coordinates $(x, y, z) = (2, 0, 0)$ centimeters and with an initial angle of 0 (horizontal). This exercise leads to the pen falling onto the lower finger and slipping to the side it is offset to, leading to contact with the upper finger as it rotates around the bottom one. As this happens, the friction from the slippage on both fingers brings the pen to a stop.

The angular acceleration estimated in equation (4.3) is compared to the true angular acceleration of the pen so as to assess the accuracy of the estimation being made. Given the exercise, meaningful angular accelerations are observed at the moment of contact, marked by a black vertical line in Figure 4.3, at around 0.11 seconds.

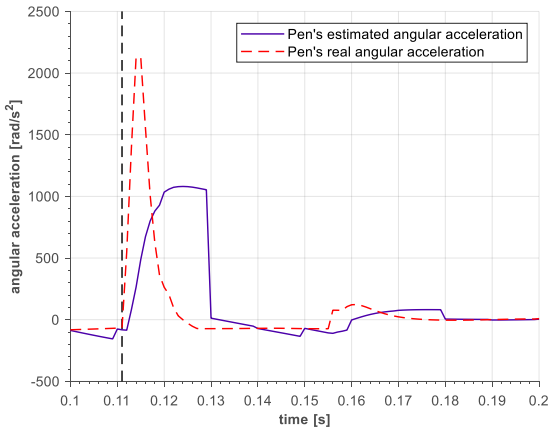

Figure 4.3 – Estimation of the pen's angular acceleration and its real angular acceleration, compared. In black, a vertical line illustrates when contact takes place.

Analyzing Figure 4.3, it is clear that the estimated pen's angular acceleration roughly follows its true angular acceleration. When the true angular acceleration has very high values though, or when these values have a high rate of change, the estimated angular acceleration does not match the true values well. The impact of this mismatch on the prediction of the pen's position is heavy, illustrated in the next figure.

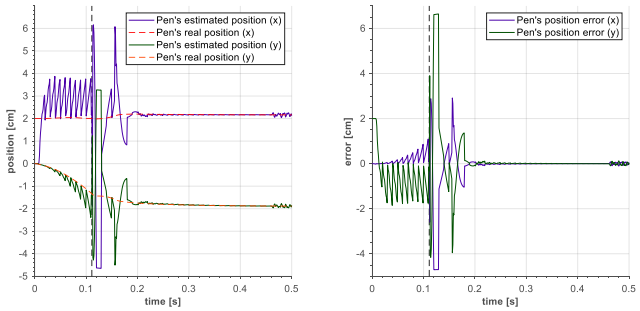

Figure 4.4 – Estimation of the position of the pen using its estimated angular acceleration. On the left, the pen's estimated position and real position. On the right, the pen's position error. In black, a vertical line illustrates when contact takes place.

Regarding the estimated angle of the pen, it can be estimated smoothly throughout the whole event, as it is not computed from the estimated angular acceleration.

5 CONTROLLER

The purpose of the controller is to make the pen oscillate from side to side, in between the fingers. The goal is for this oscillation to be a smooth movement. For this to be feasible, the grasping force on the pen cannot either be too much, as it would restrict the pen's movement, nor too little, as it would lead to the pen slipping off its grasp.

In this section a controller is introduced that is composed of three parts. These parts consist of a controller for the finger's position, an impedance controller for stable grasping and an object manipulation controller. The first two controllers produce a control action of force that, summed, represent the control action of force, applied on the finger joints. The third controller produces an action of torque, applied to the wrist.

5.1 Finger position control

The control of the position of the fingers is essentially needed to keep the fingers close and equidistant to the wrist's axis of rotation, as well as to dissipate energy associated with the movement of the fingers. Towards this end, the center-point of the fingers, $(r - r')/2$, is controlled as a critically damped system and the radial velocity of the fingers, $\dot{r}$ and $\dot{r}'$, is fed back negatively. Thus, the control action for the upper finger is given as

$$F_1 = K_{p,f}\left(r_r - \frac{(r - r')}{2}\right) + K_{d,f}\left(\dot{r}_r - \frac{(\dot{r} - \dot{r}')}{2}\right) - K_{v,f}\,\dot{r}, \qquad (5.1)$$

with equivalent control for the lower one, where r_r and $\dot{r}_r$ are the reference position and velocity for the center-point of the fingers, respectively, which are set to zero as it is intended that the finger's center-point be positioned on the wrist's axis of rotation. $K_{p,f}$, $K_{d,f}$ and $K_{v,f}$ are the control gains regarding the position and velocity of the center-point of the fingers and velocity of the fingers, respectively. Consider the displacement of the center point due to gravity alone. Then, for an allowable deviation from the wrist's axis of rotation of about 0.5 millimeters, K_p can be calculated such that

$$K_{p,f}(5 \times 10^{-4}) = (m_p + 2m_f)g, \qquad (5.2)$$

where m_p is the pen's mass, m_f is the mass of one finger and g is the acceleration of gravity. Assuming that the system is linear, this results in a control gain of $K_{p,f} \approx 729$, from which follows for a critical damping $K_{d,f} = 2(m_p + 2m_f)\sqrt{\frac{K_{p,f}}{m_p + 2m_f}} = 10.4$. Lastly $K_{v,f}$ was determined experimentally, resulting in $K_v = 10$.

5.2 Stable grasping impedance

For stable grasping, there needs to be a grasping force such that the frictional force between the pen and the fingers is enough to not let the pen slip but not too much that it overly restricts the pen's movement. The control action employed for this task, for the upper finger, consists in a proportional control where a reference penetrating distance on the pen is set [9], given as

$$F_2 = -K_{p,\delta}(\delta_r - \hat{\delta}), \qquad (5.3)$$

where δ_r is a reference value for the penetrating distance and $K_{p,\delta}$ is a control gain. The current estimated penetrating distance, $\hat{\delta}$, is calculated according to the pen's estimated position, $\hat{\boldsymbol{p}}_1$. Equivalent control action is used for the lower finger.

Consider now an exercise where the pen is held vertically between the fingers, such that the only force

counter acting the pen's weight is the frictional force, resulting in

$$F_t = m_p g, \tag{5.4}$$

where m_p is the pen's mass and g is the gravity constant. Splitting the frictional force, so that each finger is applying half of this force on the pen and considering the state of dynamic friction between the bodies (as it is the least stable state), then the normal force to be applied on the pen by each finger is

$$F_n = \frac{m_p g}{2\mu_d}. \tag{5.5}$$

Now, the penetration distance equivalent to such normal force, δ^*, can be obtained from equation (2.1), in stationarity $\dot{\delta} = 0$, therefore $K(\dot{\delta}) = k$, yielding

$$\delta^* = \sqrt[a]{\frac{1}{k}\frac{mg}{2\mu_d}}, \tag{5.6}$$

resulting in $\delta^* \approx 5.2 \times 10^{-5}$. Then, by choosing suitable values for the reference of the penetrating distance δ_r and the control gain $K_{p,\delta}$, an optimum grasping force can be reached. That said, setting $\delta_r = 8 \times 10^{-5}$, $K_{p,\delta}$ can be calculated from

$$\frac{mg}{2\mu_d} = K_{p,\delta}(\delta_r - \delta^*), \tag{5.7}$$

resulting in $K_{p,\delta} \approx 2.63 \times 10^3$.

5.3 Object manipulation impedance

The manipulation of the object, adapted from [9], is intended towards the object's angle. In such case, the dynamics of the object are governed by

$$T + T_{ext} = I_{z,p}\ddot{q} \tag{5.8}$$

where T is the manipulation torque exerted on the object by the fingertips, T_{ext} is an external perturbation torque and $I_{z,p}$ is the actual inertia of the pen. The desired interaction of the system is given as

$$T_{ext} = I_{z,d}\ddot{q} + D_T(\dot{q} - \dot{q}_r) + K_T(q - q_r) \tag{5.9}$$

where q_r and $\dot{q}_r$ are the reference angular trajectory, $I_{z,d}$ is the desired apparent inertia and D_T, K_T are the damping and stiffness, respectively. As described in [9], by keeping the inertia unchanged, $I_{z,d} = I_{z,p}$. Then, since $T_{ext} = I_{z,p}\,\ddot{q} - T$, the impedance control law is

$$T = K_T(q_r - \hat{q}) + D_T(\dot{q}_r - \dot{\hat{q}}) \tag{5.10}$$

The control gains were manually tuned, set at $K_T = 10$ and $D_T = 0$, as the presence of overshoot in the angle of the pen is actually beneficial for this task (oscillation of the pen) and therefore no damping is required.

5.4 Analysis and discussion

The control action can then be summed up as a force of grasp for the upper and lower fingers, $F = F_1 + F_2$ and $F' = F_1' + F_2'$, respectively, and a torque for the wrist, T. The system was then given a reference signal for the pen's angle, q, corresponding to a sine wave of amplitude $A = 0.7$ and frequency $\omega = 19\ rad/s$. The pen's starting position was the origin with mass center along z_0. The controlled action was recorded and is displayed in Figure 5.1, below.

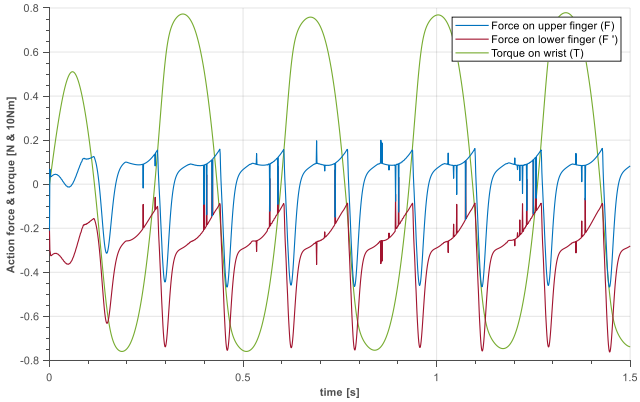

Figure 5.1 – Controller action to follow the reference of a sine wave of amplitude of $A = 0.7$ and frequency $\omega = 19\ rad/s$. The positive direction of torque is anti-clockwise and a positive force on the fingers equates to the opening of the finger, while the negative force equates to the closing of the finger.

6 SYSTEM'S RESPONSE ANALYSIS AND EXPLORATION

For the analysis of the system's response, it is important to define the phases of the rotation cycle. In Figure 6.1, these phases are depicted.

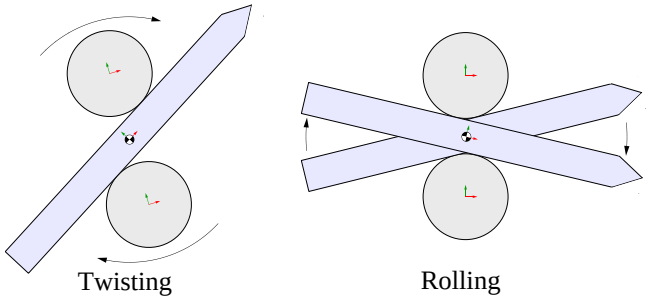

Figure 6.1 – Representation of a half-cycle of the pen oscillation movement on the fingers. On the left, negative twisting, on the right, negative rolling. The next half-cycle of the movement would consist of these same two movements, in the positive direction of rotation.

The phases in a cycle are four: negative twisting, negative rolling, positive twisting, and positive rolling. This movement is similar in each half-cycle, where the only difference is the direction of the movement. In the twisting phase the fingers apply a torque on the pen which forces is to change the direction of its rotation and begin to spin. In the rolling phase, the fingers apply a small amount of torque and let the pen spin freely.

6.1 Linearized system analysis

A simplification of the system was performed with the intent of calculating the system's resonant frequency, through its linearization. This simplified system is depicted in Figure 6.2, considered to have an imposed trajectory on the wrist's rotation, θ, as a harmonic oscillator.

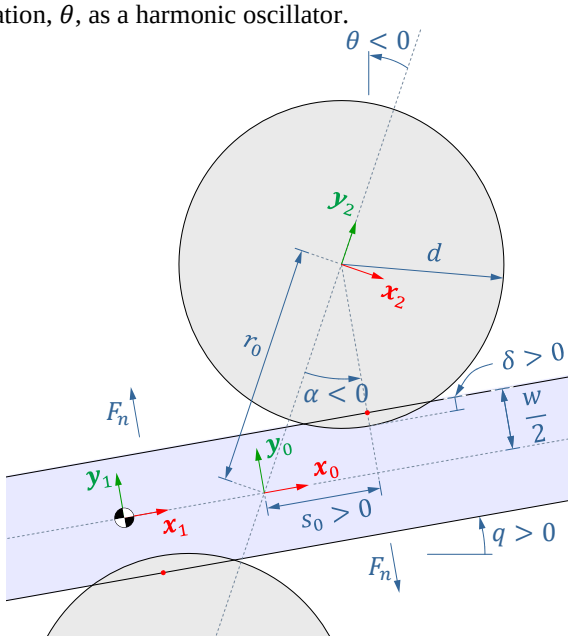

Figure 6.2 – Representation of important variables for the simplified system.

The dynamics between the pen and the fingers can be equated as

$$I_{z,p}\ddot{q} = -2\, s_0\, F_n, \tag{6.1}$$

where F_n is the normal force, as stated in (2.1), in the simplified form of

$$F_n = Ke^{\eta\dot{\delta}}\delta^a. \tag{6.2}$$

From Figure 6.2, with some manipulation, the system can be written as only a function of α, as

$$I_{z,p}\ddot{q} = 2\,K\,r_0 \sin(\alpha)\, e^{\eta\, r_0 \sin(\alpha)\dot{\alpha}} \left(d + \frac{w}{2} - r_0\cos(\alpha)\right)^a, \tag{6.3}$$

By linearizing the system around $\alpha = 0$, the first term of Taylor series will be

$$\tilde{\tau} = \left.\frac{\partial \tau}{\partial \alpha}\right|_{\alpha=0} \alpha = 2\,K\,r_0 \left(d + \frac{w}{2} - r_0\right)^a \alpha \tag{6.4}$$

with $\alpha = \theta - q$. Bearing in mind $\ddot{q} = -\omega_r^2\, q$ is the solution to a harmonic oscillator, and $\theta = 0$ in this linearization, then $q = -\alpha$ and

$$\ddot{q} = \omega_r^2\, \alpha \tag{6.5}$$

from which results, by substitution in (6.4),

$$\omega_r = \sqrt{\frac{2\,K\,r_0\left(d + \frac{w}{2} - r_0\right)^a}{I_{z,p}}} = \sqrt{\frac{2\,K\,\left(d + \frac{w}{2} - \delta\right)\delta^a}{I_{z,p}}}. \tag{6.6}$$

The resonant frequency, ω_r, can then be calculated by using mean values for the penetration distance δ. It varies with the frequency, with values between $6 \times 10^{-5}\ m$ to $8 \times 10^{-5}\ m$. This results in a resonant frequency for the system of 18.3 rad/s to 22.7 rad/s.

6.2 Frequency response

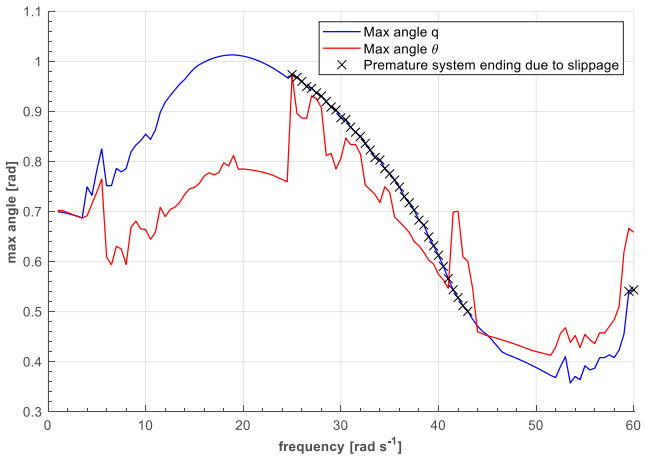

Figure 6.3 – Response of the system to a reference input on the pen's angle of a sine wave of amplitude $A = 0.7$ and frequency of ω, ranging from 1 to 60 rad/s, simulated for 5 seconds. The pen's absolute value of maximum angle, q_{max}, is drawn in blue, while the wrist's absolute value of its maximum angle, θ_{max}, is drawn in red. Black crosses are also illustrated, representing frequencies at which the system ended prematurely due to the pen slipping off the fingertips' grasp.

The system was evaluated through a range of frequencies, from 1 to 60 rad/s and an amplitude of 0.7. Its response was analyzed and the pen's maximum angle q_{max} as well as the hand's maximum angle θ_{max}, in absolute value, were recorded. Figure 6.3 illustrates the systems response to such frequencies.

At frequencies of 4 to 25 rad/s the pen begins to oscillate, as is possible to see in Figure 6.3, by the difference in value between both lines. This maximum values for the pen's rotation, q_{max}, steadily increase with the increase in frequency, achieving a maximum at around 19 rad/s, found to be the resonant frequency of the system.

At frequencies larger than 25 rad/s, the system becomes unstable, depicted in Figure 6.3 by black crosses on the frequency level at which the system let the pen escape its grasp. To note that the progressive increase of the frequency results in the lowering of q_{max}, which is a direct result of the system operating at a higher frequency than its resonant one.

Curiously, at frequencies of about 45 rad/s, the system becomes stable once again. However, $\theta_{max} > q_{max}$, and they are both much lower than they were at the resonant frequency.

6.3 Cyclical behavior analysis

To analyze the periodicity of the system, at frequencies ranging from 4 to 20 rad/s, the parametric plotting of some

key variables is of great value. Given the periodic response of the system, the following parametric plot has a period equal to two cycles of the input forced reference frequency, $\Delta t = 4\pi/\omega$.

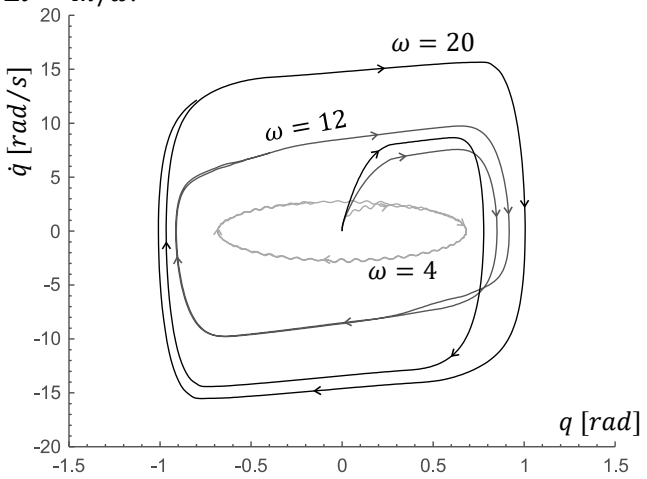

Figure 6.4 – Parametric plot of the pen's angle q and the pen's angular velocity $\dot{q}$. Three different system responses are plotted at three different input frequencies, 4, 12 and 20 rad/s. The responses were recorded over a time period of $4\pi/\omega$ of the input frequency.

From Figure 6.4, the parametric plot has a square shape through all three frequencies and the successive cycles reinforce the square shape, meaning cyclical behavior was reached [19]. The impact of the input frequency on the system is very noticeable. An increase in the input frequency equates to faster and more abrupt twisting and rolling phases, evident in the straightness of the shape's edges as the frequency increases. The maximum values for the angle and angular velocity, q and $\dot{q}$, increase as well, indicating larger and faster oscillations.

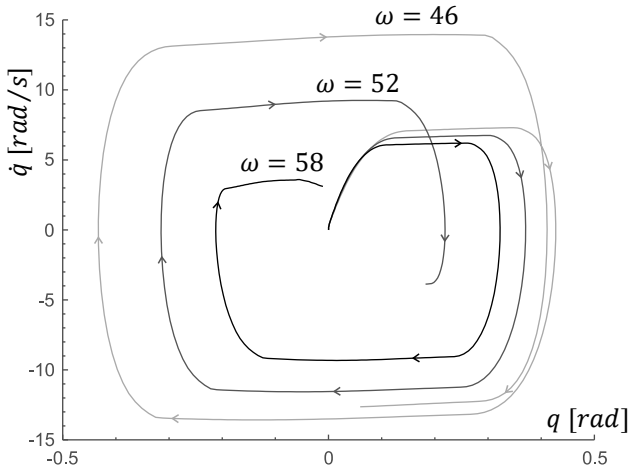

Figure 6.5 – Parametric plot of the pen's angle q and the pen's angular velocity $\dot{q}$. Three different system responses are plotted at three different input frequencies, 46, 52 and 58 rad/s. The responses were recorded over a time period of $4\pi/\omega$ of the input frequency.

At higher frequencies of 46 to 58 rad/s, the response of the system evolves so as to decrease the magnitude of oscillation, $q - \theta$, as had been observed in Figure 6.3. On a parametric plot of the pen's angle and angular velocity, Figure 6.5, the system's responses are still distinguishable from each other and the inverse of Figure 6.4 can be observed, where the higher the input frequency is, the lesser the impact on q and $\dot{q}$.

It is also noticeable that, although the same period of two cycles of the input reference frequency was recorded, the pen only went through one cycle of rotation, indicating that the system is running at a frequency higher than the pen's dynamics allow and suggesting the presence of period doubling [20, 21], a phenomenon where a new periodic trajectory emerges from the already existing periodic trajectory. Investigating this phenomenon further, at the input frequency of 58 rad/s, the relevant parametric plot can be seen in Figure 6.6.

In Figure 6.6, period doubling is clearly present, evident in the v-shave created in the plot. This shape takes form because the pen's dynamics do not allow it to oscillate at the frequency at hand. The presence of a large magnitude of oscillation is also verified, as per the "openness" of the shape in the plot, meaning that the rolling phase is very prevalent. There is little to no evidence of both angles moving in synchrony, indicating that the twisting phase is very short lived. The pen's angle does stay within bounds though, and the plot is cyclical, proving the system is stable for the frequency at hand. All in all, at high frequencies, the pen is limited to the rolling phase while being juggled between the fingers at a frequency higher than its resonant frequency.

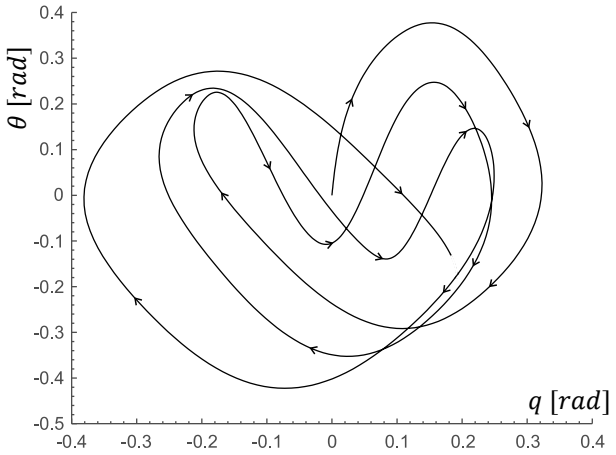

Figure 6.6 – Parametric plot of the pen's angle q and the wrist's angle θ, at the frequency of 58 rad/s. The response was recorded over a time period of $12\pi/\omega$ (6 cycles) of the input frequency.

7 CONCLUSIONS

7.1 Achievements

This document goes into detail about how the act of grasping is sensed by the bio-mechanisms of human biology and how a robotic hand can be controlled to perform a task in which an object, a pen, is grasped and handled to perform a wiggling motion in between the fingertips. The controller was given a

reference signal to follow of a sine wave with a given amplitude and frequency. It proved quite effective at using the guidance of the reference to oscillate the pen, managing to maintain stability while operating at the resonant frequency of the system, of about 19 rad/s. The system's response was analyzed regarding the frequency of the reference input signal. At frequencies of 4 to 25 rad/s the pen begins to oscillate and at 45 to 58 rad/s, the phenomenon of period doubling can be observed.

7.2 Future work

One of the main aspects this essay enables is the addition of inbound and outbound delays to the system model, similar to its biological counterpart [16], to better simulate a true bio-inspired mechanism. This implementation is expected to be complex, as a delay of over 100 milliseconds should be enough to cause the pen to slip the fingertips' grasp.

Furthermore, this model hopes to inspire the study of various forms of dexterous movement involving the handling of objects with a non-restrictive grasp and clever use of the fingers to perform complex movements with said objects.

8 REFERENCES

[1] R. W. Shumaker, K. R. Walkup and B. B. Beck, Animal tool behavior: the use and manufacture of tools by animals, JHU Press, 2011.

[2] J. L. Bradshaw, "Animal asymmetry and human heredity: Dextrality, tool use and language in evolution–10 years after Walker (1980)," *British Journal of Psychology,* pp. 39-59, 1991.

[3] S. R. James, "Hominid use of fire in the Lower and Middle Pleistocene: A review of the evidence [and comments and replies]," *Current Anthropology,* pp. 1-26, 1989.

[4] K. S. Brown, "Fire as an Engineering Tool of Early Modern Humans," *Science,* pp. 859-862, 2009.

[5] T. Matsuzawa, "Primate foundations of human intelligence: a view of tool use in nonhuman primates and fossil hominids.," *Primate origins of human cognition and behavior,* pp. 3-25, 2008.

[6] R. A. Foley and R. Lewin, Principles of human evolution, John Wiley & Sons, 2013.

[7] S. KADOWAKI, "Issues of chronological and geographical distributions of Middle and Upper Palaeolithic cultural variability in the Levant and implications for the learning behavior of Neanderthals and Homo sapiens.," *Dynamics of Learning in Neanderthals and Modern Humans Volume 1,* pp. 59-91, 2013.

[8] S. A. A. Moosavian and E. Papadopoulos, "Multiple Impedance Control for Object Manipulation," *Proceedings. 1998 IEEE/RSJ International Conference on Intelligent Robots and Systems. Innovations in Theory, Practice and Applications (Cat. No. 98CH36190),* pp. 461-466, October 1998.

[9] M. Li, H. Yin, K. Tahara and A. Billard, "Learning Object-level Impedance Control for Robust Grasping and Dexterous Manipulation," *2014 IEEE International Conference on Robotics and Automation,* pp. 6784-6791, May 2014.

[10] D. J. Balkcom and M. T. Mason, "Robotic origami folding," *The International Journal of Robotics Research,* pp. 613-627, 2008.

[11] A. S. Carvalho and J. M. Martins, "Exact restitution and generalizations for the Hunt-Crossley contact model," *Mechanism and Machine Theory,* 17 March 2019.

[12] H. Geyer and H. Herr, "A Muscle-Reflex Model That Encodes Principles of Legged Mechanics Produces Human Walking Dynamics and Muscle Activities," *IEEE Transactions on neural systems and rehabilitation engineering,* pp. 263-273, June 2010.

[13] E. Pennestrì, V. Rossi and P. Salvini, "Review and comparison of dry friction force models," *Nonlinear dynamics,* pp. 1785-1801, 21 July 2015.

[14] M. Zhang and A. F. T. Mak, "Prosthetics and Orthotics International," *In vivo friction properties of human skin,* 1999.

[15] S. Derler, R. Huber, H. P. Feuz and M. Hadad, "Influence of surface microstructure on the sliding friction of plantar skin against hard substrates.," *Wear,* pp. 1281-1288, 2009.

[16] E. R. Kandel, J. H. Schwartz, T. M. Jessell, S. A. Siegelbaum and A. J. Hudspeth, Principles of Neural Science, New York: McGraw-hill, 2000.

[17] E. R. Baldwin, P. M. Klakowicz and D. F. Collins, "Wide-pulse-width, high-frequency neuromuscular stimulation: implications for functional electrical stimulation.," *Journal of Applied Physiology,* pp. 228-240, 2006.

[18] C. Donnely, "Modulation of torque evoked by wide-pulse, high-frequency neuromuscular electrical stimulation and the potential implications for rehabilitation and training," *Scientific Reports,* pp. 1-13, 2021.

[19] S. A. Campbell, "Limit cycles, tori, and complex dynamics in a second-order differential equation with delayed negative feedback.," *Journal of Dynamics and Differential Equations,* pp. 213-236, 1995.

[20] C. Tresset, P. Coullet and E. de Faria, "Period doubling," *Scholarpedia,* p. 3958, 2014.

[21] D. W. Jordan and P. Smith, Nonlinear ordinary differential equations: an introduction to dynamical systems., USA: Oxford University Press, 1999.